

High-Speed SICM for the Visualization of Nanoscale Dynamic Structural Changes in Hippocampal Neurons

Yasufumi Takahashi,^{*,†,‡,§} Yuanshu Zhou,[†] Takafumi Miyamoto,[§] Hiroki Higashi,[§]
Noritaka Nakamichi,^{||} Yuka Takeda,^{||} Yukio Kato,^{||} Yuri Korchev,^{†,⊥,¶} and Takeshi Fukuma[†]

[†]WPI Nano Life Science Institute (WPI-NanoLSI), Kanazawa University, Kanazawa 920-1192, Japan

[‡]Precursory Research for Embryonic Science and Technology (PRESTO), Japan Science and Technology Agency (JST), Saitama 332-0012, Japan

[§]Department Division of Electrical Engineering and Computer Science, Kanazawa University, Kanazawa 920-1192, Japan

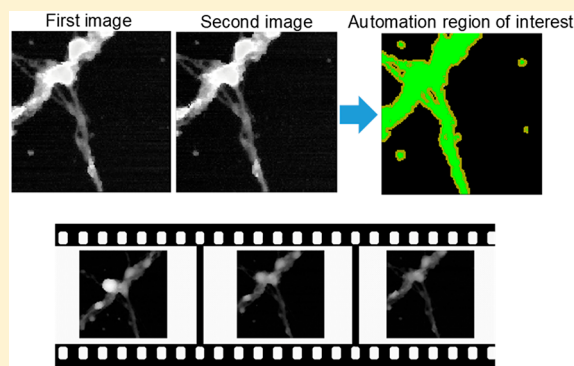
^{||}Faculty of Pharmacy, Institute of Medical, Pharmaceutical and Health Sciences, Kanazawa University, Kanazawa 920-1192, Japan

[⊥]Department of Medicine, Imperial College London, London W12 0NN, United Kingdom

[¶]National University of Science and Technology (MISiS), Leninskiy prospect 4, Moscow 119049, Russia

Supporting Information

ABSTRACT: Dynamic reassembly of the cytoskeleton and structural changes represented by dendritic spines, cargo transport, and synapse formation are closely related to memory. However, the visualization of the nanoscale topography is challenging because of the diffraction limit of optical microscopy. Scanning ion conductance microscopy (SICM) is an effective tool for visualizing the nanoscale topography changes of the cell surface without labeling. The temporal resolution of SICM is a critical issue of live-cell time-lapse imaging. Here, we developed a new scanning method, automation region of interest (AR)-mode SICM, to select the next imaging region by predicting the location of a cell, thus improving the scanning speed of time-lapse imaging. The newly developed algorithm reduced the scanning time by half. The time-lapse images provided not only novel information about nanoscale structural changes but also quantitative information on the dendritic spine and synaptic bouton volume changes and formation process of the neural network that are closely related to memory. Furthermore, translocation of plasmalemmal precursor vesicles (ppvs), for which fluorescent labeling has not been established, were also visualized along with the rearrangement of the cytoskeleton at the growth cone.



Dynamic reassembly of the cytoskeleton and structural changes represented by dendritic spines,¹ cargo transport,² and synapse formation³ are closely related to memory.^{4,5} Two-photon excitation microscopy allows for the stimulation and observation of samples by using a caged compound and has been used to reveal the relationship between neurotransmitters and changes in synapse volume at the single-synapse level.¹ Fluorescence microscopy is a useful tool for characterizing dynamic structural changes. However, in some cases, the relatively large size of the fused fluorescent proteins and the photoinduced cell damage can disturb membrane trafficking. Despite the recent development of the receptor-selective small-molecule labeling technology,⁶ the estimation of the nanoscale height and volume changes of live neurons remains difficult. Therefore, a nonlabeling topography imaging technology is required to understand the relationship between rearrangement of the cytoskeleton and neuronal function.

Scanning ion conductance microscopy (SICM) is a unique and promising technique for capturing live-cell nanoscale topographical dynamic changes under physiological condi-

tions.^{7–14} SICM uses a nanopipette as a probe to monitor an ionic current between an electrode placed inside the pipet and an electrode located in a bath, as a feedback signal for controlling the nanopipette–sample distance. SICM has been used to characterize neuronal topography and local function, e.g., ion-channel and active-potential measurement using topographical information to navigate the nanopipette at a specific region.^{15–17} However, the temporal resolution of conventional SICM is not suitable for time-lapse imaging. As a high-speed imaging modality of scanning probe microscopy, fast-scan atomic force microscopy is also used for imaging hippocampal neurons.¹⁸ Nevertheless, even if these techniques are available, tracing the dynamic topographical changes of the spine, bouton, and growth cone remains challenging because of the microscale steep vertical slope of neurites.

Received: October 19, 2019

Accepted: December 16, 2019

Published: December 16, 2019



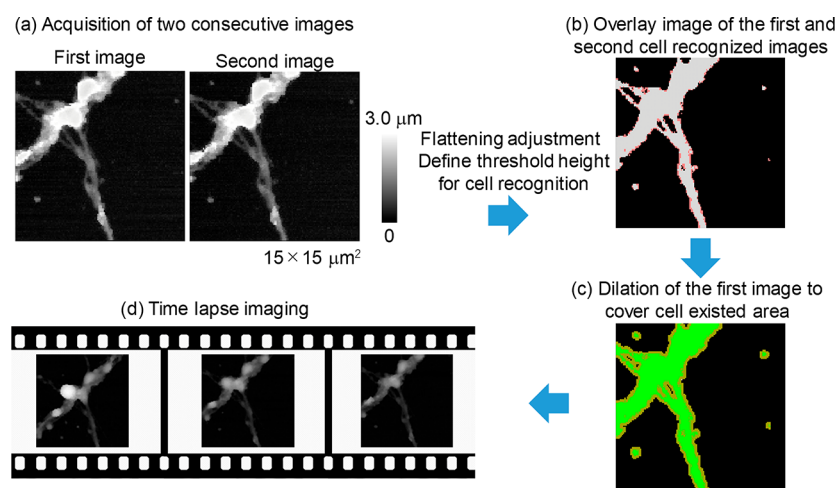


Figure 1. (a) Principles of automation region of interest (AR)-mode SICM. (b) Overlay of two continuous SICM topography images. (c) Flesh was placed on the first image to cover the second cell-containing region by optimizing the parameter for the AR-mode. (d) Time-lapse imaging of a hippocampal neuron. The scan size was $15 \times 15 \mu\text{m}^2$.

The development of hardware for SICM is important for the improvement of its temporal resolution. Particularly, in the case of hopping-mode SICM, overshoot caused by a delay of the Z-axis piezo during the falling leads to sample deformation, which is critical for the measurement of fragile nanoscale cavities or protrusions. To prevent this undesirable deformation and improve temporal resolution, the dual Z piezo actuator system was developed.¹⁹ An additional small high-resonant-frequency piezo actuator attached to the Z-axis piezo actuator is used to keep the nanopipette away from the sample instantaneously when it reaches the sample's surface. Similarly, Tilman and co-workers developed a turn-step protocol for subsecond speed imaging.¹⁰ To improve the speed of the movement of the piezo stage, small-capacitance and high-resonant-frequency piezo stages are also effective.^{20,21}

The scanning method is a key element for improving temporal resolution because the feedback control cannot predict the height of the scanned region in advance. In particular, the imaging of structures with a high aspect ratio is challenging. In the case of neurons, for instance, this is because these cells have a narrow dendrite and a large cell body. Hopping-mode SICM, in which the probe approaches and withdraws from the sample's surface during repetitive scanning, is a promising method for imaging the topography of living cells without contact.^{17,22,23} However, the hopping mode is time-consuming compared with conventional lateral scanning. Novak and co-workers solved this problem by changing pixel size during measurements using prescanning.¹⁷ We developed an algorithm for optimizing the hopping amplitude during scanning and minimizing these unnecessary movements for revealing the nanoscale dynamics of microvilli.²⁰ However, this scanning algorithm has a slight possibility of collision. Therefore, it is limited in terms of the scanning of the surface of a fragile sample with a floating structure, such as the dendritic spines of neurons.

Here, we have developed automation region of interest (AR)-mode SICM and a fast Z-axis scanner for improving the temporal resolution of topography imaging. The newly developed algorithm requires half of the scanning time and allows for the visualization of dynamic cargo transport, changes in the volume of dendritic spines and synaptic boutons, and the growth cones of hippocampal neurons without labeling.

MATERIALS AND METHODS

SICM Setup. The SICM setup was as described in the Supporting Information and our previous report.²⁸ The glass nanopipettes (aperture inner radius, 50 nm) were fabricated from a borosilicate glass capillary (GC100F-15, Harvard Apparatus) using a CO₂ laser puller (model P-2000, Sutter Instruments). The nanopipettes were filled with the same sample-immersion solution, and Ag/AgCl electrodes were inserted into them. The applied voltage (−0.2 V) generated an ionic flow through the tip as a feedback signal.

To visualize the morphological dynamics of neurons, we developed a homemade high-resonance-frequency Z-piezo stage. The capacitance and resonance frequency of the piezo stages were 0.75 μF and 30 kHz, respectively. We developed a new algorithm, the automation region of interested (AR) mode, for high-speed scanning aimed at selecting the scanning area using the previous topography image (Figure 1a).

The ion current was measured using a homemade 1 GΩ feedback resistance current amplifier. The probe was placed close to the sample by using a stepping motor (KXC06020-GC, SURUGA SEIKI) and the homemade Z-piezo stage. The stepping motor with the Z-piezo stage was positioned on a manually operated XYZ manipulator (BSS76–60C, SURUGA SEIKI) with a travel range of ±6.5 mm. The precise probe position was controlled by XY- and Z-piezo stages. The scanning algorithms were controlled by a program written using LabVIEW2014 (National Instruments). The field-programmable gate array (National Instruments, NI USB-7856 OEM) was compiled using programs developed by us. The measurement signals were collected and all equipment was controlled. The measurement part of this system was constructed on an optical microscope (Nikon, ECLIPSE Ti-S) placed on an antivibration table (Herz, TS-150).

The parameters of the hopping mode are described in detail herein. The hopping amplitude was 1–3 μm. The waiting time after lateral movement was 1 ms. During this time, a reference current, I_{REF} , was measured as the average of the DC current through the probe. The probe falling and withdrawing speed was 150–320 and 1200 nm/ms, respectively. The set point was 99.7%–99.3% of I_{REF} .

Preparation of Hippocampal Neurons. Pregnant ICR mice were purchased from Japan SLC (Hamamatsu, Japan)

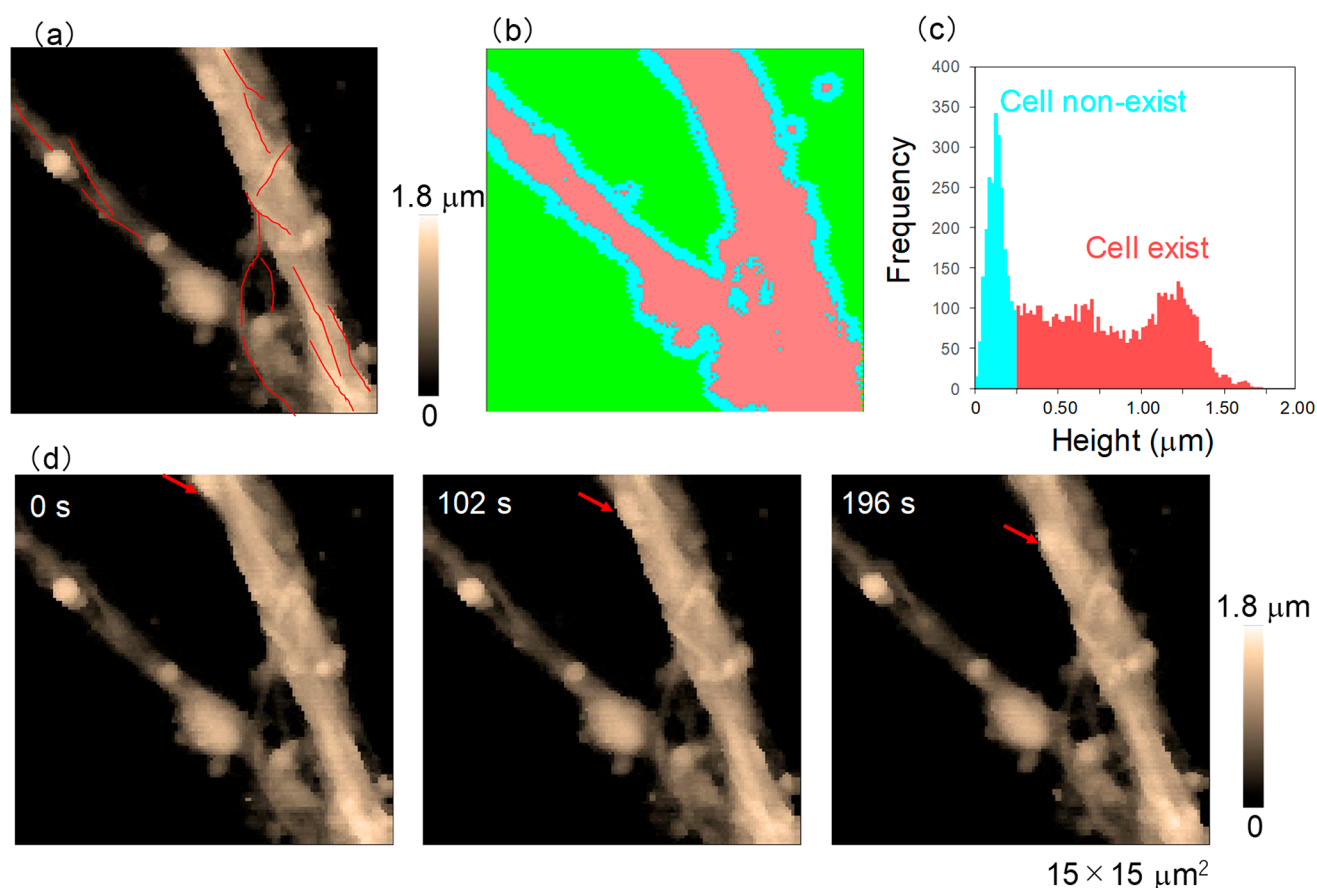


Figure 2. (a) AR-mode SICM image of the topography of a dendrite of a hippocampal neuron. The red lines indicate the position of microtubule bundles. (b) The neuron-containing, noncontaining, and without scanning regions are labeled in red, blue, and green, respectively. (c) Histogram of the height of topography images. (d) Time-lapse AR-mode images of cargo transport (red arrows) in the dendrites of a hippocampal neuron. The scan size was $15 \times 15 \mu\text{m}^2$.

and used for neuronal culture. The mice were housed under pathogen-free conditions at controlled temperature (21–25 °C) with a 12 h light/dark cycle. The lights remained on from 8:00 to 20:00, and food and water were available ad libitum. The animals were cared for in strict compliance with the guidelines outlined in the National Institutes of Health Guide for the Care and Use of Laboratory Animals. All animal procedures used in this work were approved by the Kanazawa University Animal Care Committee. Primary hippocampal neuronal cultures were prepared according to the method of Nakamichi, with minor modifications.³⁴ In brief, hippocampi from 15-day-old embryonic ICR mice were dissected and incubated with 0.25% trypsin in phosphate-buffered saline containing 28 mM glucose at 37 °C for 20 min. Cells were mechanically dissociated using a 1000 μL pipet tip in culture medium and plated at a density of 1.5×10^4 cells/cm² on cover glasses (Matsunami glass, Osaka, Japan) coated with 7.5 μg/mL poly-L-lysine in a 4 well dish (Thermo Fisher Scientific, Waltham, MA). Hippocampal neurons were cultured in B-27 Electrophysiology Kit (Thermo Fisher Scientific, Waltham, MA) supplemented with penicillin (100 U/mL), streptomycin (100 μg/mL), glutamine (0.5 mM), and glutamate (25 μM) during the initial 3 days at 37 °C in a humidified 5% CO₂ incubator. Thereafter, half of the culture medium was replaced with B-27 Electrophysiology Kit supplemented with penicillin (100 U/mL), streptomycin (100 μg/mL), and glutamine (0.5 mM) every 3 days.

RESULTS AND DISCUSSION

To capture nanoscale dynamic structural changes, we developed an AR mode that allows for the selection of the next imaging region by predicting the location of a cell from a previous image. The AR mode is a useful scanning method for visualizing neuronal topographical changes because it saves the scanning pixels and eliminates the physical contact between the nanopipette and the sample.

The first step of AR-mode SICM was the acquisition of two consecutive images and determination of the parameters for defining the height threshold and for distinguishing a cell from the substrate, so as to identify the location of the cell. Subsequently, we predicted cell location and selected the scanning region. To identify the location of cells and select the scanning area, to save scanning time, three parameters (plane fit, height threshold, and image dilation) were used. The plane-fit parameter is used to correct sample tilt. We used the X and Y constant slope offset to cancel the tilt. Height threshold (typically 250 nm) is used to identify the sample's height. The setting of the plane-fit parameter is important to avoid the misidentification of the cells and the substrate because of the tilt. The image-dilation parameter is used to identify the location of the cell in the first image, to follow the change in shape from the first image to the second image. This process is effective in predicting structural changes and saves scanning time by selecting the scanning region around the cell.

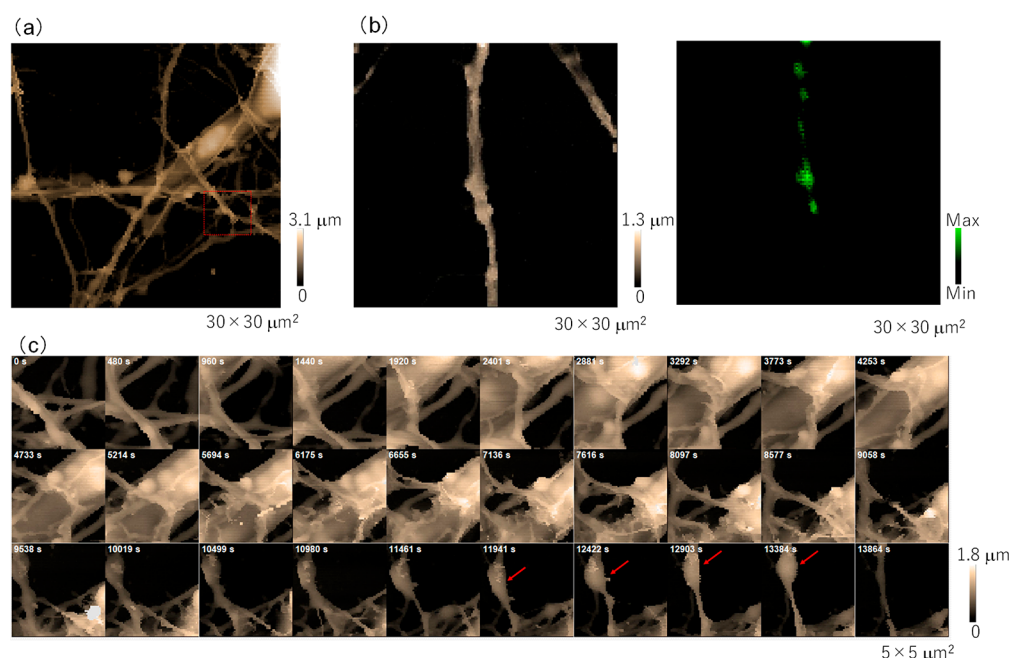


Figure 3. (a) Low-magnification SICM topography image of a dendrite. (b) SICM (left) topography and (right) confocal microscopy images. Mitochondria were stained using MitoTracker Green FM. (c) High-magnification SICM time-lapse images of a dendrite. The scanned area is indicated by the red square in Figure 3(a). The scan size was (a) $30 \times 30 \mu\text{m}^2$, (b) $30 \times 30 \mu\text{m}^2$, and (c) $5 \times 5 \mu\text{m}^2$.

As an example of the parameter setting of the AR mode, Figure 1 shows consecutive images of a hippocampal neuron. The two consecutive images are shown in Figure 1a and an overlay image of the area where the cells are present in two consecutive images is shown in Figure 1b. The gray part of Figure 1b depicts cells that were identified in both images, whereas the red part depicts nonoverlapping areas in the two images because of cell movement. Then, the first image was fleshed out to follow the area in which the cells moved during the second imaging. Figure 1c shows the fleshing treatment of the first image (yellowish green) and the overlay of the first and second images (green). In this case, the region containing the second cell was followed using AR-mode SICM. The fleshing treatment was effective in selecting the region containing the cell and saving scanning time. In some cases, the AR-mode was not able to capture the topography of the whole sample, e.g., changes in the shape of cells that exceeded the region predicted from previous images or the appearance in the image of structures from outside the imaging range during time-lapse imaging. To avoid such situations, it is necessary to compare several successive images and adjust each measurement, to cope with changes sufficiently.

To explain the effect of the AR-mode in saving scanning time, Figure 2 and Supporting Movie 1 show the AR-mode SICM images of a dendrite of a hippocampal neuron at 16 days in vitro (DIV). One of the sequential topography images obtained using AR-mode SICM was selected and divided into three regions: the nonscanned region (green), scanned region without cells (blue), and scanned region with cells (red; Figure 2a,b). Figure 2c shows the histogram of the height data from Figure 2a. Based on the tricolor image, we confirmed that the AR-selected scanning area covered the cell-containing region without losing cell structure. The number of pixels of the nonscanned region, scanned region without cells, and scanned region with cells was 8475, 2318, and 5591, respectively. The scanning time of the AR-mode and of the conventional

scanning mode (first captured image for parameter setting) was 98 and 239 s, respectively. The maximum height difference was $<2.0 \mu\text{m}$. Within the scanning area, we found that the regions with a height of $<250 \text{ nm}$ and the regions with a height of $>250 \text{ nm}$ were regions without cells and regions with cells, respectively; this coloring was also adopted in the histogram. The ratio of scanning pixels without cells was 29.3% in this scanning region. This result implies that AR-mode SICM can effectively reduce the scanning time by selecting the scanning region during time-lapse imaging without losing structural information.

SICM was used to visualize directly the dense bundles of microtubules on dendrites without labeling. To identify these microtubules, we used red lines on the microtubule bundle in the topography image (Figure 2a). These shape and length values fitted the results of previous research on microtubules.²⁴ Using AR-mode SICM imaging, we could also visualize directly the cargo transport on the bundles of microtubules as a surface topography change without labeling (Supporting Movie 1 and red arrows in Figure 2d), which was mediated by motor proteins.²

To investigate the cargo transport in greater detail, we performed high-magnification imaging of neurites. To select the region containing the neurites, we imaged a relatively large-scale neurite of a hippocampal neuron. Figure 3 shows low- and high-magnification SICM time-lapse topography images of the hippocampal neuron at 4 DIV. We selected the region marked by the red square in the low-magnification image of Figure 3a to perform high-magnification time-lapse SICM imaging. The pixel size was 64×64 and we did not use the AR-mode in this measurement, because there were only a few regions in which the pixels did not correspond to cells. The average imaging time was 68 s/image. Supporting Movie 2 shows the captured dynamic topography of a neurite. To confirm the molecule that mediated cargo transport, we performed SICM and confocal microscopy simultaneously. We

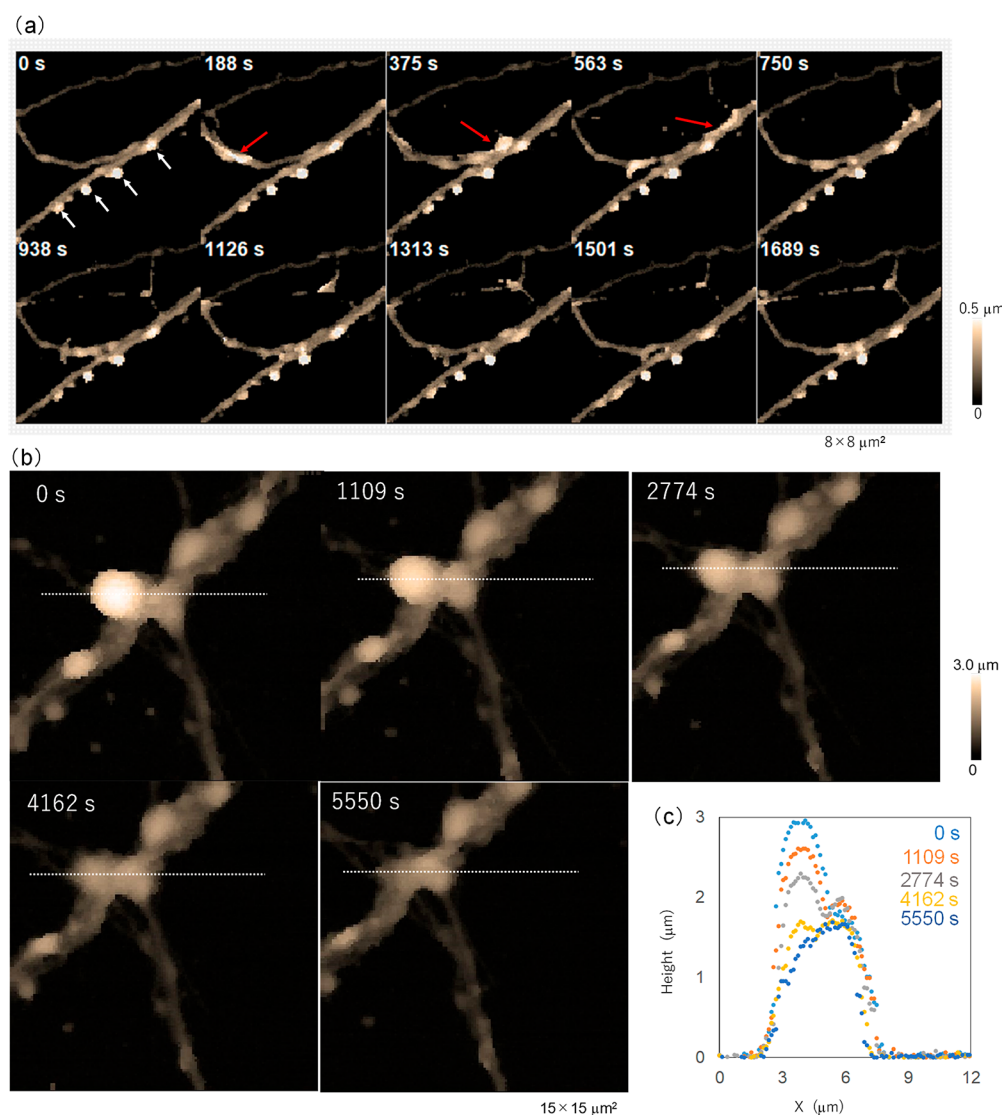


Figure 4. AR-mode SICM topographic images of (a) dendritic spine and synaptic network formation and (b) volume change in synaptic boutons. (c) Cross-section image of a synaptic bouton. The area where cross-section was performed is indicated by the dotted line in panel a. The scan size was (a) $8 \times 8 \mu\text{m}^2$ and (b) $15 \times 15 \mu\text{m}^2$.

observed a similar structure in the fluorescence image of a mitochondria-containing region. Based on these results, we propose that the cargo transport observed in this experiment was mitochondria-mediated transport. The speed of the cargo transport was estimated as being $0.011 \mu\text{m/s}$, as assessed using the time-lapse images (red arrows in Figure 3c), which was slower than the value reported previously, $0.91 \pm 0.26 \mu\text{m/s}$.²⁵ Although we improved the scanning speed, the SICM imaging speed remained insufficient for evaluating the fast cargo transport. However, cargo transport speed is correlated with the cell-maturation state and the type of cell. Therefore, in this experiment, some mitochondria with low motility were captured by SICM.²⁶

Dendritic spines and synaptic boutons are also important targets for super-resolution microscopy because of their submicroscale shape and volume change, which are related to their function.²⁷ We visualized the structure of dendritic spines using high-speed SICM. Figure 4a and Supporting Movie 3 show the time-lapse imaging of relatively mature neurons at 14 DIV. We visualized protrusions from dendrites that appeared to be dendritic spines (white arrows in Figure

4a). The height and width of the spiny structures, as evaluated using the topography image, were 700 and 500 nm, respectively. Cargo transport was also observed (Supporting Movie 3). Around the synaptic bouton or varicosity, we observed the formation of a neural network. The dynamic reassembly of actin filaments and actin wave-like propagation were observed (red arrows in Figure 4a) just before this event.

Changes in synaptic bouton structure were also visualized by SICM. Figure 4b and Supporting Movie 4 show the time-lapse imaging of neurons at 17 DIV. The volume and size of the synaptic bouton, which is indicated by the red arrow in Figure 4b, decreased spontaneously with time. Figure 4c and Supporting Movie 4 show the cross-section of the synaptic bouton. The initial height of the bouton (3 μm) decreased to 1.5 μm . The time scale of such long-term dynamics of the synaptic bouton was in accordance with the results of a previous report based on super-resolution microscopy.²⁷

To underscore the importance of high-resonance-frequency Z piezo for the noncontact imaging of neurons, we also performed SICM imaging using a Z-axis piezo with a relatively low resonance frequency (6.2 kHz). To evaluate the current

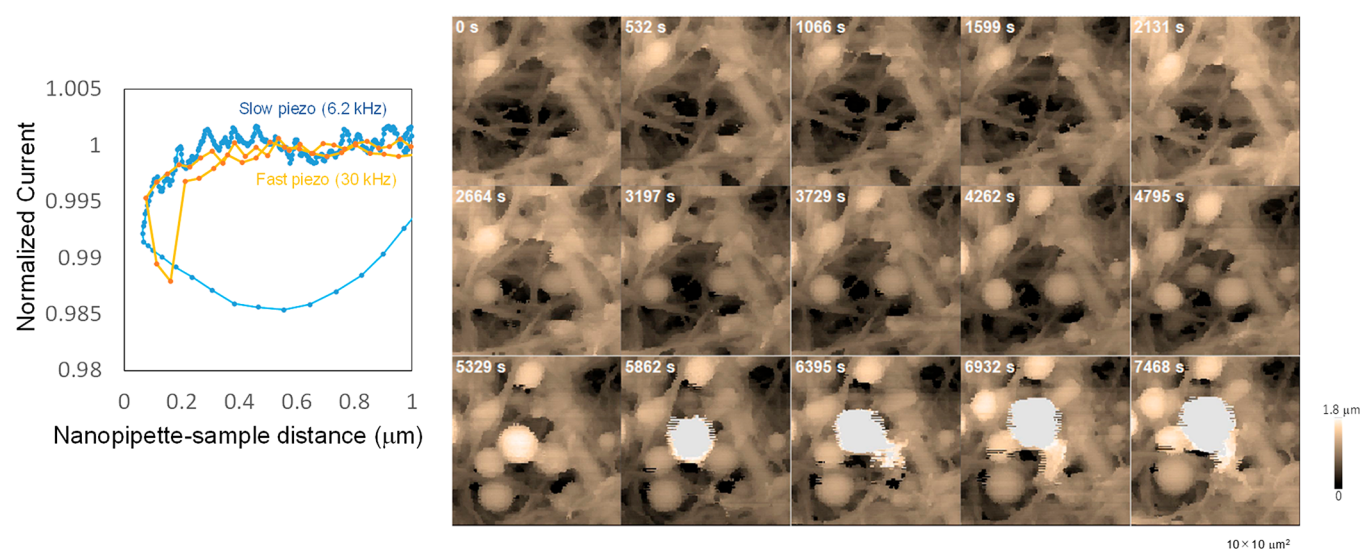


Figure 5. (a) SICM characteristic of fast (30 kHz) and slow (6.2 kHz) resonant-frequency piezo stage and (b) SICM topography images of nanopipette–sample contact-induced bleb formation on neurites. The scan size was $10 \times 10 \mu\text{m}^2$.

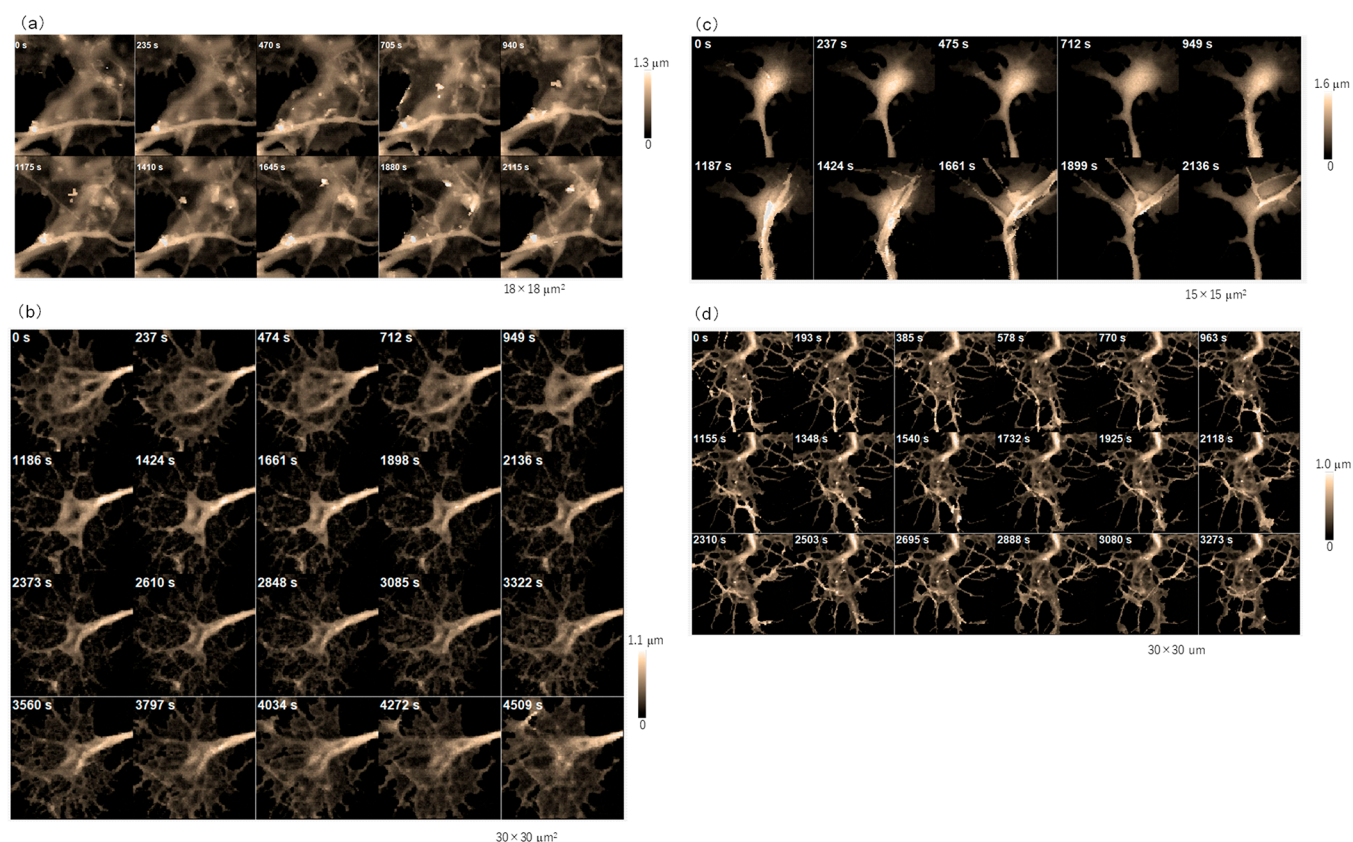


Figure 6. Dynamic cytoskeleton rearrangement in a growth cone. (a) Quick expansion of the P domain. (b) Synchronized shrinking of lamellipodia. (c) Actin-bundle formation. (d) Cargo transport at the growth cone. The scan sizes were (a) $18 \times 18 \mu\text{m}^2$, (b) $30 \times 30 \mu\text{m}^2$, (c) $15 \times 15 \mu\text{m}^2$, and (d) $30 \times 30 \mu\text{m}^2$.

and distance relationship, Figure 5 and Supporting Movie 5 show the approach characteristic of relatively slow and fast Z piezo stage for live neurons. The falling/withdrawing speed of slow and fast Z piezo stages were 50/900 and 240/1200 nm/ms, respectively. The sampling rate of the current and distance signals was 10 kHz. The height was calculated by applying voltage to the Z piezo stage. In the case of the slow Z piezo stage, the height position of the nanopipette was overshoot

immediately after changing to the withdrawal process, and the current decreased for 0.6 ms. In the case of fast Z piezo stage, the current decrease was observed only 0.2 ms after the change in the nanopipette from approaching to withdrawing. The Z piezo stage overshoot led to contact between the nanopipette and the sample and induced stress in the live neuron. During the time-lapse imaging of neurons at 16 DIV using the slow Z piezo stage, we observed the formation of blebs that were

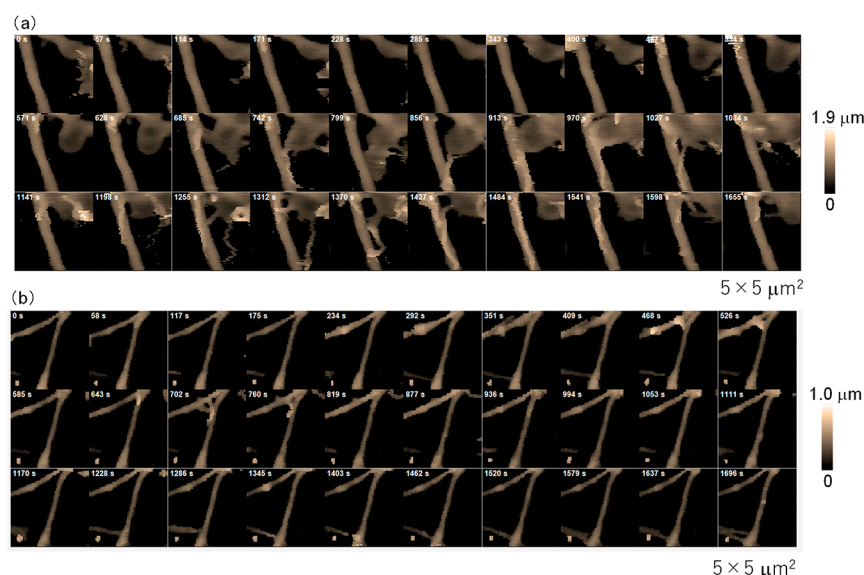


Figure 7. Visualization of synapse formation. (a) Lamellipodia- and (b) filopodia-like structures formed and created the synapse. The scan sizes were $5 \times 5 \mu\text{m}^2$ and $5 \times 5 \mu\text{m}^2$, respectively.

induced by the force stress imparted by the physical interaction between the nanopipette and the sample. Previously, we discussed the guidelines of SICM for noncontact topography imaging.²⁸ Using a fast Z piezo stage is important for the performance of high-speed noncontact imaging in keeping with the guidelines because of the overshoot problem of Z piezo stages, especially to visualize the fragile hippocampal neurons.

Next, we observed the dynamic rearrangement of the cytoskeleton at the growth cone. Growth cones contain several cytoskeletal components that are organized into three regions: the peripheral (P) domain, the transitional (T) domain, and the central (C) domain. The P domain is primarily composed of unipolar actin filament bundles embedded in a less polar actin network. It contains dynamic lamellipodia and filopodia. Microtubules are also transiently found within this domain. Using the high-speed SICM, we observed the spontaneous extension of the P domain in neurons at 7 DIV (Figure 6a and Supporting Movie 6). The contracted P domain structure returned to its original state within 135 s. We also observed that the lamellipodia present at the P domain contracted with synchronization with the surrounding lamellipodia structure of neurons at 2 DIV (Figure 6b and Supporting Movie 7). The contracted P domain protruded from the spreading branches of actin filaments and returned to the original state. A wave of dynamic reorganization of actin bundles was also observed in neurons at 1 DIV (Figure 6c and Supporting Movie 8).^{29–31} Cargo transport was also observed frequently (Figure 6d and Supporting Movie 9), because the plasmalemmal precursor vesicles (ppvs) were transported to maintain the vastly expanded surface, which required continuous addition of new membranes.⁴ However, due to the lack of specific biochemical markers, functional experiments that link ppvs to plasmalemmal expansion have been conducted using pulse-labeling strategies, to identify the vesicles that were synthesized most recently. SICM is an effective tool for such ppvs-related dynamics of cargo transport because it can visualize the changes in surface structure related to ppvs transportation without labeling.

The synapse-formation process is also a good application for SICM because the size of neurites is close to the diffraction

limit. To visualize synapse formation using SICM, we performed high-magnification and low-pixel (64×64) imaging at the neurite. In these experiments, we did not use the AR-mode because the filopodia sometimes appeared outside the initial scanning area. Figure 7a and Supporting Movie 10 show the time-lapse images of the neurites of neurons at 17 DIV. A sheet-like structure appeared in the middle part of the dendrite and elongated to touch the neighboring dendrite. Subsequently, filopodia formed from the sheet-like structure and adhered to the closest neurite. The filopodium–neurite connection, with elongation of filopodia and retraction of neurons at 10 DIV, was also visualized by SICM (Figure 7b and Supporting Movie 11). The filopodia touched the same spot on the neurite several times and formed a synapse. The process of synapse formation observed here agrees with the filopodial model.³² SICM was a useful tool to characterize submicroscale topography changes, such as synapse formation, without labeling.

CONCLUSION

We developed AR-mode SICM to improve the temporal resolution of SICM by selecting the scanning area during time-lapse measurements. Using AR-mode SICM, we have halved the scanning time and been able to directly visualize dendritic spine and synaptic bouton volume changes, dynamic translocation of plasmalemmal precursor vesicles (ppvs) and synchronized shrinking phenomena of P domain at the growth cone, and synapse formation process. The nanoscale SICM images visualized not only the cargo molecule transport phenomena but also dynamic rearrangement of the cytoskeleton, bundles of actin filaments and microtubules. In neurons, the lack of a satisfactory biomarker and the adverse effects of overexpressed fluorescent protein are issues that have limited our understanding of the mechanism of cargo transport. SICM is able to visualize intrinsic neuron behavior without using fluorescent proteins. The confocal microscopy–SICM hybrid system was effective in identifying organelles and characterizing the relationship between topography and the rearrangement of organelle distribution within cells. SICM was also a highly useful tool to collect the cytosol or organelles within

cells for analyzing mRNA localization.³³ In the future, this technique is expected to identify the organelles during scanning and hence to enable the subsequent analysis of the mRNA of individual cargo-transport vesicles.

■ ASSOCIATED CONTENT

● Supporting Information

The Supporting Information is available free of charge at <https://pubs.acs.org/doi/10.1021/acs.analchem.9b04775>.

Details of the SICM setup and scheme of a homemade SICM system (DOCX)

Movie showing SICM images of a dendrite of a hippocampal neuron at 16 days in vitro (MP4)

Movie showing captured dynamic topography of a neurite (MP4)

Movie showing the time-lapse imaging of relatively mature neurons at 14 DIV (MP4)

Movie showing the time-lapse imaging of neurons at 17 DIV (MP4)

Movie showing the approach characteristic of relatively slow and fast Z piezo stage for live neurons (MP4)

Movie showing the spontaneous extension of the P domain in neurons at 7 DIV (MP4)

Movie showing the lamellipodia present at the P domain contracted with synchronization with the surrounding lamellipodia structure of neurons at 2 DIV (MP4)

Movie showing a wave of dynamic reorganization of actin bundles observed in neurons at 1 DIV (MP4)

Movie showing cargo transport (MP4)

Movie showing the time-lapse images of the neurites of neurons at 17 DIV (MP4)

Movie showing the filopodium–neurite connection, with elongation of filopodia and retraction of neurons at 10 DIV (MP4)

■ AUTHOR INFORMATION

Corresponding Author

*E-mail: yasufumi@se.kanazawa-u.ac.jp.

ORCID

Yasufumi Takahashi: 0000-0003-2834-8300

Takeshi Fukuma: 0000-0001-8971-6002

Author Contributions

Y.T., Y.Z., T.M., and H.H. performed the experiments and collected the data. N.N. and Y.T. prepared sample. Y.T. developed software of AR mode SICM. Y.T., Y.K., Y.K., and T.F. wrote the manuscript. All authors read and approved the manuscript.

Notes

The authors declare no competing financial interest.

■ ACKNOWLEDGMENTS

This work was supported by World Premier International Research Center Initiative (WPI) from MEXT, Japan. Development of Systems and Technology for Advanced Measurement and Analysis from AMED (The Japan Agency for Medical Research and Development)-SENTAN; PRESTO (JPMJPR14FA) from the Japan Science and Technology Agency (JST); a Grant-in-Aid for Scientific Research (A) (19H00993), a Grant-in-Aid for Scientific Research (B) (15H04664), a Grant-in-Aid for Scientific Research (C) (19K07126), a Grant-in-Aid for Young Scientists (A)

(15H05422), and a Grant-in-Aid for Young Scientists (19K15601) from the Japan Society for the Promotion of Science (JSPS). Y.T. was supported by Kurita Water and Environment Foundation; Mitani foundation for research and development; the foundation for the Promotion of ion engineering; Nakatani foundation; Novartis research foundation; CASIO science promotion foundation. Y.K. was supported by Biotechnology and Biological Sciences Research Council. The authors would also like to thank Mr. Naoto Matsumura for preparation of primary hippocampal neuronal cultures. Y.K. acknowledges Russian Science Foundation (Grant No. 19-19-00626) for supporting the work related to development of the concept of high speed SICM.

■ REFERENCES

- (1) Kasai, H.; Fukuda, M.; Watanabe, S.; Hayashi-Takagi, A.; Noguchi, J. *Trends Neurosci.* **2010**, *33*, 121–129.
- (2) Hirokawa, N.; Noda, Y.; Tanaka, Y.; Niwa, S. *Nat. Rev. Mol. Cell Biol.* **2009**, *10*, 682–696.
- (3) Lohmann, C.; Bonhoeffer, T. *Neuron* **2008**, *59*, 253–260.
- (4) Pfenninger, K. H. *Nat. Rev. Neurosci.* **2009**, *10*, 251–261.
- (5) Bloom, O. E.; Morgan, J. R. *Mol. Cell. Neurosci.* **2011**, *48*, 339–348.
- (6) Yamaura, K.; Kiyonaka, S.; Numata, T.; Inoue, R.; Hamachi, I. *Nat. Chem. Biol.* **2016**, *12*, 822–830.
- (7) Hansma, P. K.; Drake, B.; Marti, O.; Gould, S. A. C.; Prater, C. B. *Science* **1989**, *243*, 641–643.
- (8) Korchev, Y. E.; Bashford, C. L.; Milovanovic, M.; Vodyanoy, I.; Lab, M. J. *Biophys. J.* **1997**, *73*, 653–658.
- (9) Shevchuk, A. I.; Frolenkov, G. I.; Sanchez, D.; James, P. S.; Freedman, N.; Lab, M. J.; Jones, R.; Klenerman, D.; Korchev, Y. E. *Angew. Chem., Int. Ed.* **2006**, *45*, 2212–2216.
- (10) Simeonov, S.; Schäffer, T. E. *Nanoscale* **2019**, *11*, 8579–8587.
- (11) Seifert, J.; Rheinlaender, J.; Novak, P.; Korchev, Y. E.; Schäffer, T. E. *Langmuir* **2015**, *31*, 6807–6813.
- (12) Hagemann, P.; Gesper, A.; Happel, P. *ACS Nano* **2018**, *12*, 5807–5815.
- (13) Ushiki, T.; Nakajima, M.; Choi, M.; Cho, S.-J.; Iwata, F. *Micron* **2012**, *43*, 1390–1398.
- (14) Nakajima, M.; Mizutani, Y.; Iwata, F.; Ushiki, T. *Semin. Cell Dev. Biol.* **2018**, *73*, 125–131.
- (15) Vivekananda, U.; Novak, P.; Bello, O. D.; Korchev, Y. E.; Krishnakumar, S. S.; Volynski, K. E.; Kullmann, D. M. *Proc. Natl. Acad. Sci. U. S. A.* **2017**, *114*, 2395–2400.
- (16) Novak, P.; Gorelik, J.; Vivekananda, U.; Shevchuk, A. I.; Ermolyuk, Y. S.; Bailey, R. J.; Bushby, A. J.; Moss, G. W. J.; Rusakov, D. A.; Klenerman, D.; Kullmann, D. M.; Volynski, K. E.; Korchev, Y. E. *Neuron* **2013**, *79*, 1067–1077.
- (17) Novak, P.; Li, C.; Shevchuk, A. I.; Stepanyan, R.; Caldwell, M.; Hughes, S.; Smart, T. G.; Gorelik, J.; Ostanin, V. P.; Lab, M. J.; Moss, G. W. J.; Frolenkov, G. I.; Klenerman, D.; Korchev, Y. E. *Nat. Methods* **2009**, *6*, 279–281.
- (18) Shibata, M.; Uchihashi, T.; Ando, T.; Yasuda, R. *Sci. Rep.* **2015**, *5*, 08724 DOI: 10.1038/srep08724.
- (19) Shevchuk, A. I.; Novak, P.; Taylor, M.; Diakonov, I. A.; Ziyadeh-Isleem, A.; Bitoun, M.; Guicheney, P.; Lab, M. J.; Gorelik, J.; Merrifield, C. J.; Klenerman, D.; Korchev, Y. E. *J. Cell Biol.* **2012**, *197*, 499–508.
- (20) Ida, H.; Takahashi, Y.; Kumatani, A.; Shiku, H.; Matsue, T. *Anal. Chem.* **2017**, *89*, 6015–6020.
- (21) Watanabe, S.; Ando, T. *Appl. Phys. Lett.* **2017**, *111*, 113106.
- (22) Takahashi, Y.; Murakami, Y.; Nagamine, K.; Shiku, H.; Aoyagi, S.; Yasukawa, T.; Kanzaki, M.; Matsue, T. *Phys. Chem. Chem. Phys.* **2010**, *12*, 10012–10017.
- (23) Happel, P.; Dietzel, I. D. *J. Nanobiotechnol.* **2009**, *7*, 7.

- (24) Schatzle, P.; da Silva, M. E.; Tas, R. P.; Katrukha, E. A.; Hu, H. Y.; Wierenga, C. J.; Kapitein, L. C.; Hoogenraad, C. C. *Curr. Biol.* **2018**, *28*, 2081–2093.
- (25) MacAskill, A. F.; Rinholm, J. E.; Twelvetrees, A. E.; Arancibia-Carcamo, I. L.; Muir, J.; Fransson, A.; Aspenstrom, P.; Attwell, D.; Kittler, J. T. *Neuron* **2009**, *61*, 541–555.
- (26) Lewis, T. L., Jr.; Turi, G. F.; Kwon, S. K.; Losonczy, A.; Polleux, F. *Curr. Biol.* **2016**, *26*, 2602–2608.
- (27) Chéreau, R.; Saraceno, G. E.; Angibaud, J.; Cattaert, D.; Nägerl, U. V. *Proc. Natl. Acad. Sci. U. S. A.* **2017**, *114*, 1401–1406.
- (28) Zhou, Y. S.; Saito, M.; Miyamoto, T.; Novak, P.; Shevchuk, A. I.; Korchev, Y. E.; Fukuma, T.; Takahashi, Y. *Anal. Chem.* **2018**, *90*, 2891–2895.
- (29) Katsuno, H.; Toriyama, M.; Hosokawa, Y.; Mizuno, K.; Ikeda, K.; Sakumura, Y.; Inagaki, N. *Cell Rep.* **2015**, *12*, 648–660.
- (30) Inagaki, N.; Katsuno, H. *Trends Cell Biol.* **2017**, *27*, 515–526.
- (31) Nozumi, M.; Nakagawa, H.; Miki, H.; Takenawa, T.; Miyamoto, S. *J. Cell Sci.* **2003**, *116*, 239–246.
- (32) Yuste, R.; Bonhoeffer, T. *Nat. Rev. Neurosci.* **2004**, *5*, 24–34.
- (33) Nashimoto, Y.; Takahashi, Y.; Zhou, Y. S.; Ito, H.; Ida, H.; Ino, K.; Matsue, T.; Shiku, H. *ACS Nano* **2016**, *10*, 6915–6922.
- (34) Nakamichi, N.; Taguchi, T.; Hosotani, H.; Wakayama, T.; Shimizu, T.; Sugiura, T.; Iseki, S.; Kato, Y. *Neurochem. Int.* **2012**, *61*, 1121–1132.